Electronic Supplementary Material (ESI) for Journal of Materials Chemistry A.

Highly efficient multifunctional frosted luminescent solar concentrators with zero-energy nightscape lighting

Note S1 Structure analysis and characterization of SAO and SAON phosphors

Table S1 Chemical compositions of SAO phosphors from XPS measurements.

	Binding energy (eV)					Atomic %				
	Sr 3d	Al 2p	O 1s	Eu 3d	Dy 3d	Sr3d	Al	O	Eu	Dy
SAO	133.43	73.74	531.11	1134.19	1336.07	7.32	16.04	56.27	0.25	0.33

Table S2 Chemical compositions of SAON phosphors from XPS measurements.

	Binding energy (eV)					Atomic %				
	Si 2p	Al 2p	O 1s	N 1s	Eu 3d	Si	Al	O	N	Eu
SAON	101.39	73.6	532.11	397.03	1134.1	34.84	2.5	8.97	42.62	0.17

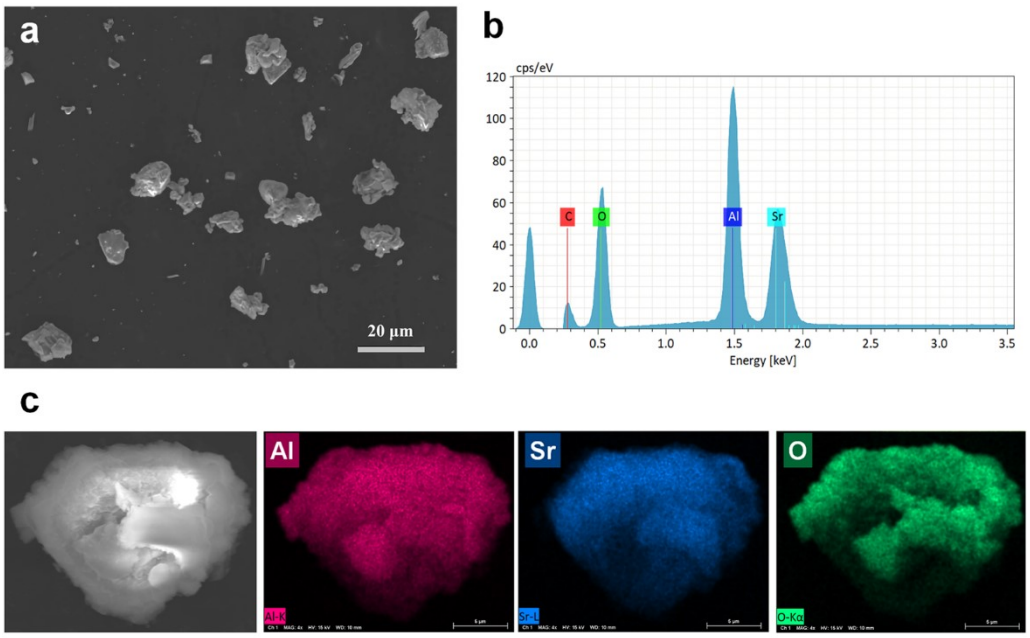

Fig. S1 Structural analysis and characterization on SAO. (a) SEM image of SAO phosphors. (b) Composition of SAO phosphors determined by EDS. (c) SAO phosphors elemental maps of Al, Sr and O.

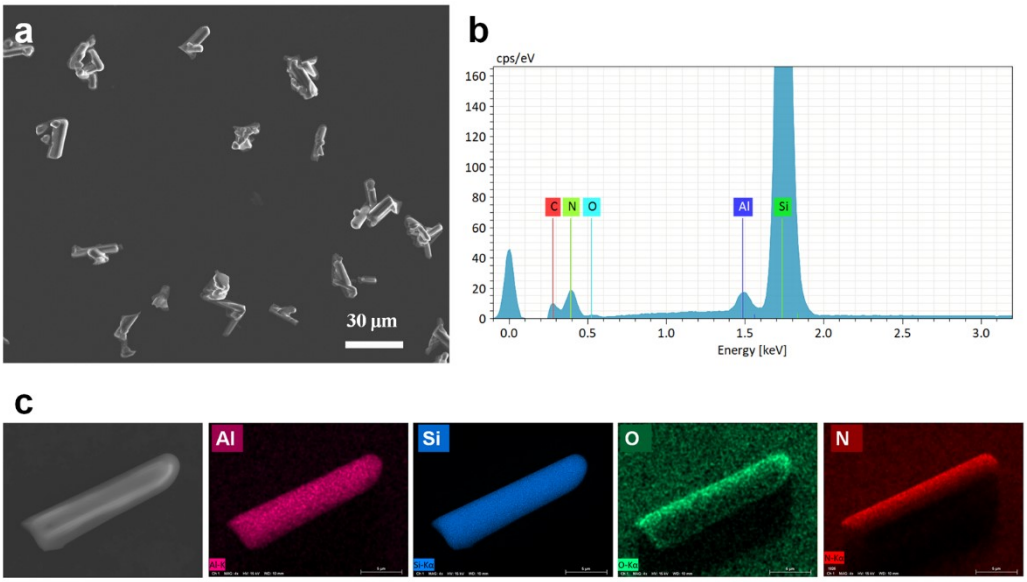

Fig. S2 Structural analysis and characterization on SAON. (a) SEM image of SAON phosphors. (b) Composition of SAON phosphors determined by EDS. (c) SAON phosphors elemental maps of Al, Si, O and N.

Note S2 The calculation of PLQY

The PLQY is defined as the ratio of the number of emitted photons to that of absorbed photons. PLQY values of phosphors are estimated by the following Eq:

$$PLQY = \frac{\int L_s d\lambda}{\int E_R d\lambda - \int E_s d\lambda} \quad \text{(S1)}$$

where $\int L_s d\lambda$, $\int E_R d\lambda$ and $\int E_s d\lambda$ represent the fluorescence integral intensities of emission, background and excitation spectrum, respectively.

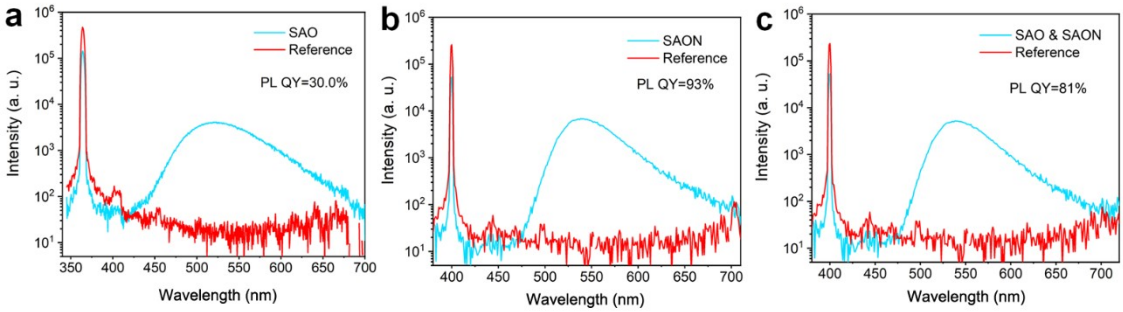

Fig. S3 PLQY of phosphors. The reference line and emission spectra of SAO (a), SAON (b), and the mixture of SAO and SAON phosphors (c). The reference line was measured by scattering the excitation on $BaSO_4$.

Note S3 UV−visible diffuse reflectance of phosphors

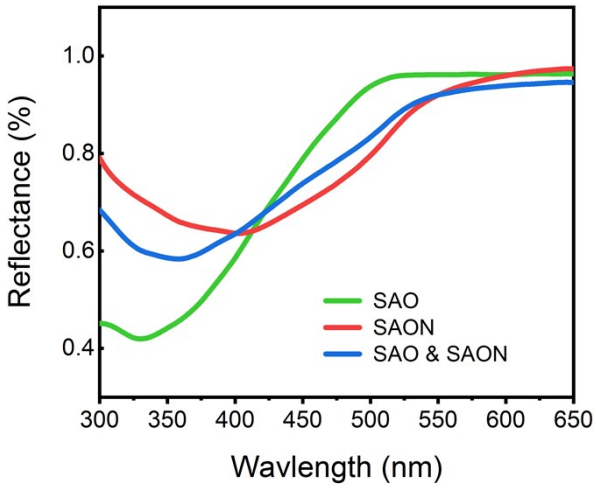

Fig. S4 Diffuse reflectance spectra of SAO, SAON and mixture phosphors.

Note S4 Schematic diagrams of the photoluminescence and persistent luminescence mechanism.

For SAON phosphors, the 4f electrons of Eu^{2+} ions are photoionized to the $5d_1$ and $5d_2$ levels of Eu^{2+} ions under excitation. Excited electrons in the $5d_2$ level relax nonradiatively to the $5d_1$ level, and contribute to green photoluminescence through the $5d_1 \rightarrow 4f$ transition (Fig. S4a). [1]

For SAO phosphors, the 4f electrons of Eu^{2+} ions are photoionized to the 5d level of Eu^{2+} ions under excitation. Parts of these electrons are subsequently captured by the traps of Dy^{3+}. Some of these electrons relax nonradiatively to the 5d level and contribute to green luminescence through the $5d_1 \rightarrow 4f$ transition of Eu^{2+} ions (Fig. S4b). [2] After terminating excitation, the captured electrons in the traps would escape with the assistance of thermal activation energy, gradually transfer back through the CB, and recombine with the ionized Eu^{2+} ions to generate green persistent luminescence (Fig. S4c).

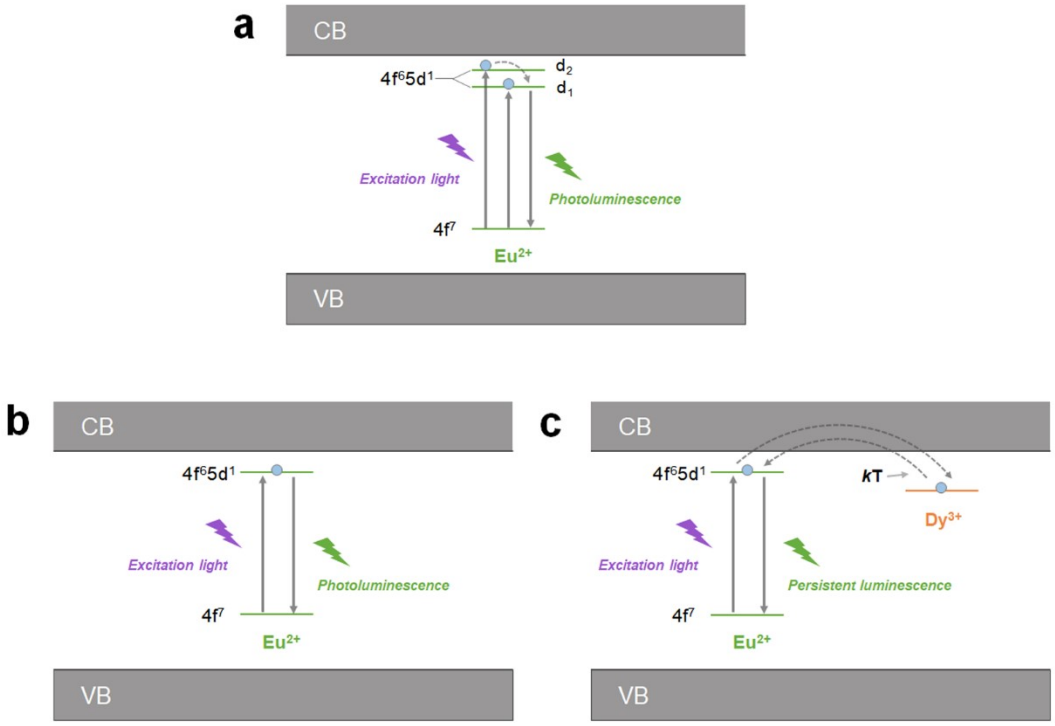

Fig. S5 Illustration of the photoluminescence and the persistent luminescence. Schematic energy level diagrams explaining photoluminescence of SAON phosphors (a), photoluminescence (b) and persistent luminescence (c) of SAO phosphors, respectively.

Note S5 The measurements of η_{edge} and PLQY of FLSCs

As shown in Fig. S6 and S7, the total PL spectrum is the emission from the entire FLSC, and the face PL spectrum is the emission of the FLSC with edges masked with black tape. The edge PL spectrum was obtained by total PL spectrum minus face PL spectrum.

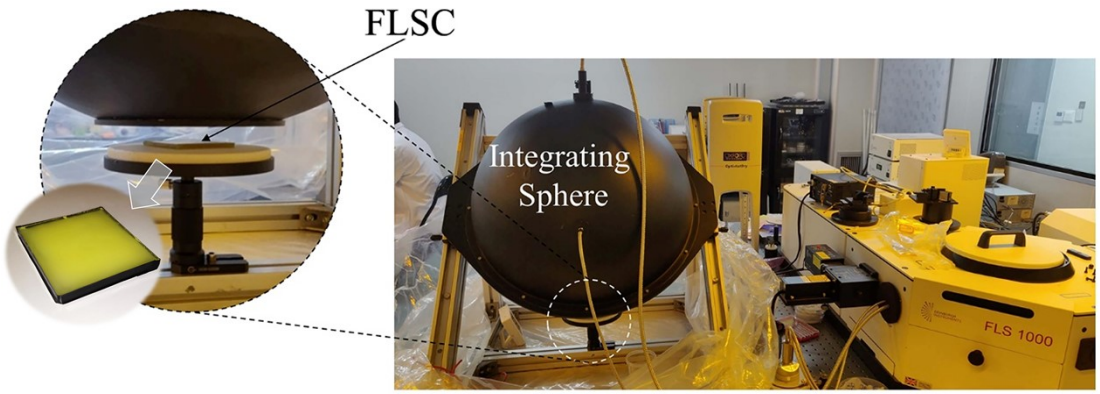

Fig. S6 The modified setup used to quantify edge-emission efficiency and PLQY of FLSCs. Photograph of an integrating sphere fiber-coupled with the FLS1000 spectrometer (Edinburgh Instruments), which was used to evaluate the optical performance of the FLSCs.

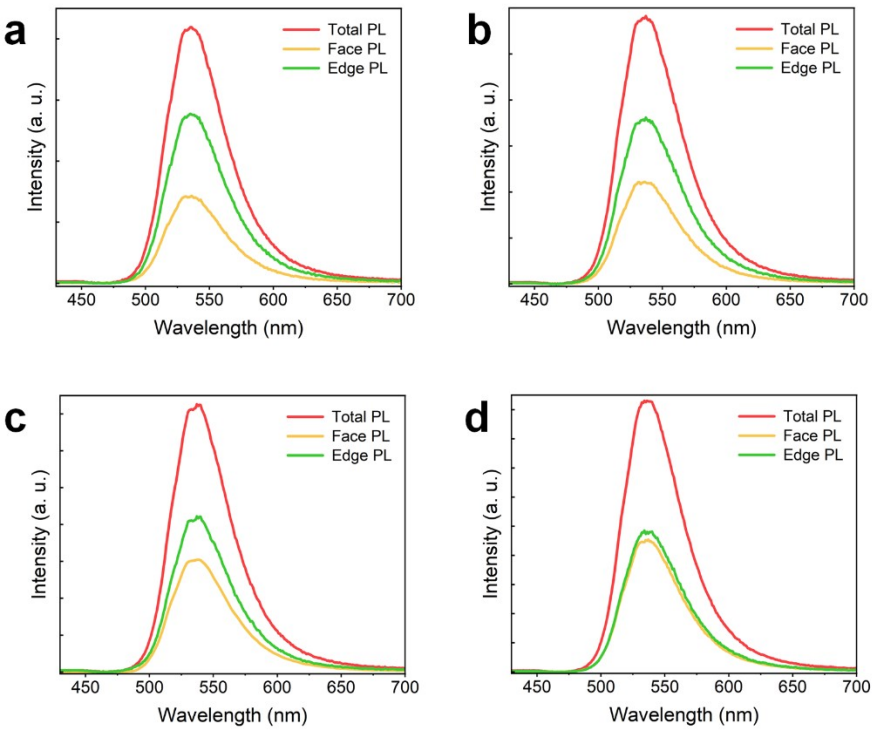

Fig. S7 Edge-emission efficiency of phosphors. Total PL spectrum, face PL spectrum and edge PL spectrum of DS1 (a), DS2 (b), DS3 (c), and DS4 (d).

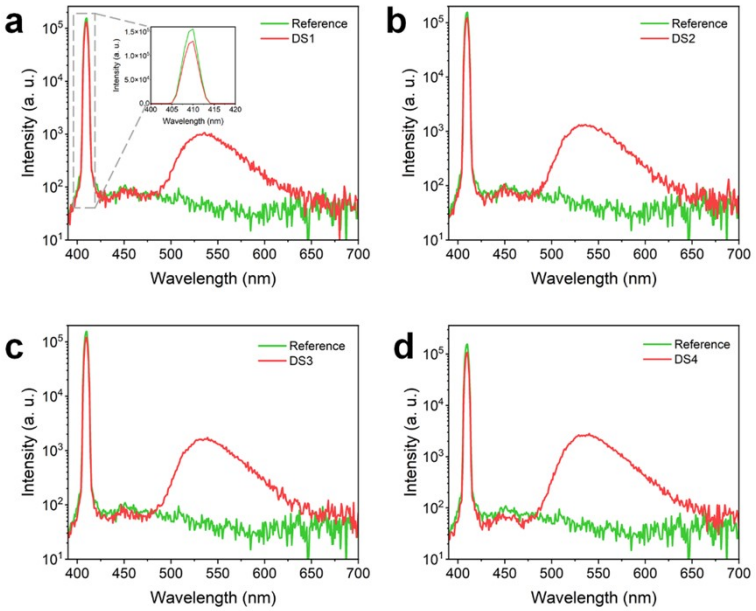

Fig. S8 PLQY of phosphors. The excitation reference line and PL spectra of DS1 (a), DS2 (b), DS3 (c), and DS4 (d).

Note S6 Monte Carlo ray-tracing simulation

Monte Carlo ray-tracing simulation is an approach of applying repeated random sampling to determine the fate of a large number of simulated rays within an LSC. [3,4] The outcomes of many events encountered by rays within the LSC are determined using random number generation weighted by calculated probabilities based on the physical properties of the system. Probabilities are assigned to light absorption, emission, non-radiative recombination, scattering, reflection and transmission from phosphors and OSTE polymer matrix materials. Simulation input parameters include the number of incident photons (50,000), the position and direction of the incident light, the size of the FLSC, the refractive index of the OSTE polymer matrix material (n=1.6) and air, the PLQY and absorption of phosphors, the PL spectra of phosphors, absorption coefficients of OSTE polymer matrix materials and phosphors, and scattering coefficient of the FLSC.

In this simulated model, FLSC components have been broken up into several general categories. The FLSC geometry consists of the following classes of objects (Fig. S9):

Boundary objects: There are three types of boundaries containing outer boundaries, inner boundaries and collected boundaries. The boundary is used to determine the behavior of the angle between the propagation direction of the photon and the boundary constrained by Snell's Law.

Particle objects: A particle object is assigned to a particle volume to handle light interaction with phosphor particles. Light interactions contain scattering, absorbing and emitting events, and the characteristics of these events are traced.

Interior objects: A interior object is used to determine the fate of scattering and absorption elements of light without encountering the particle object in the OSTE polymer matrix material. Light propagation in the OSTE polymer matrix material will inherit some characteristic of light before these events. For example, the reflected photon will inherit the random free path of the photon before reflection, but it changes the propagation direction of the photon.

Fig. S10 shows the general paths that a bundle can traverse through these objects, navigating probabilistically through the various boundaries, particles and interiors that have been created.

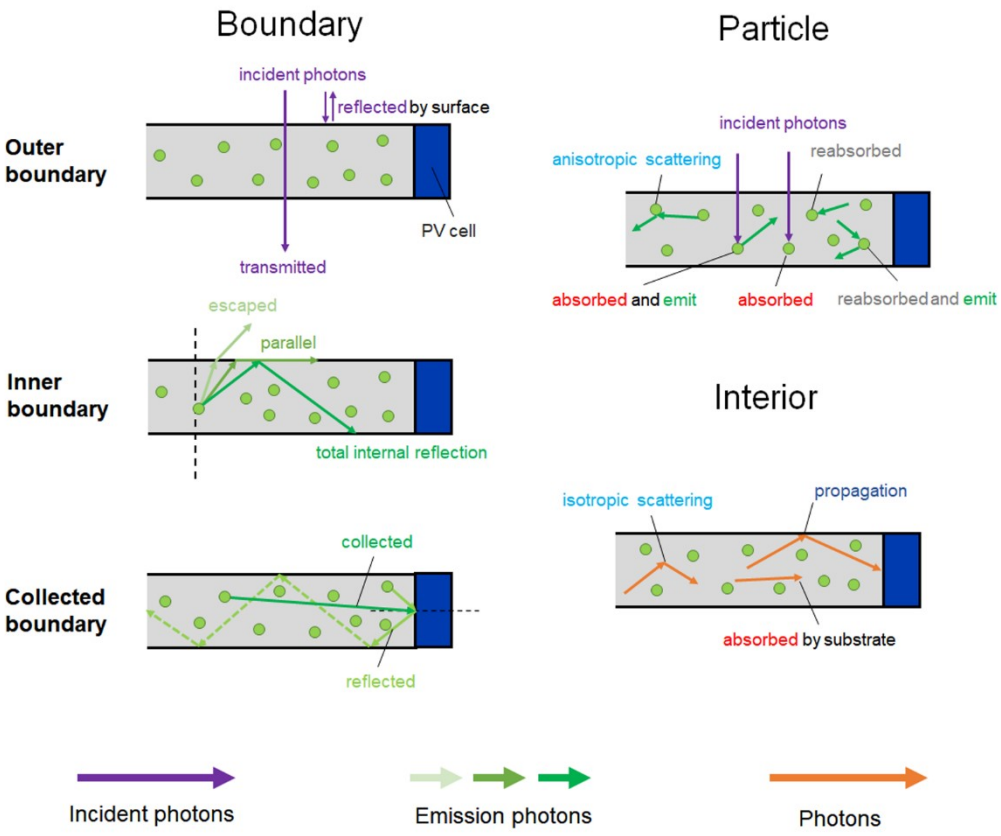

Fig. S9 Illustration of Monte Carlo ray-tracing simulated model in the FLSC. A schematic of three classes of objects (boundary, particle and interior in FLSCs) and light interactions with various objects.

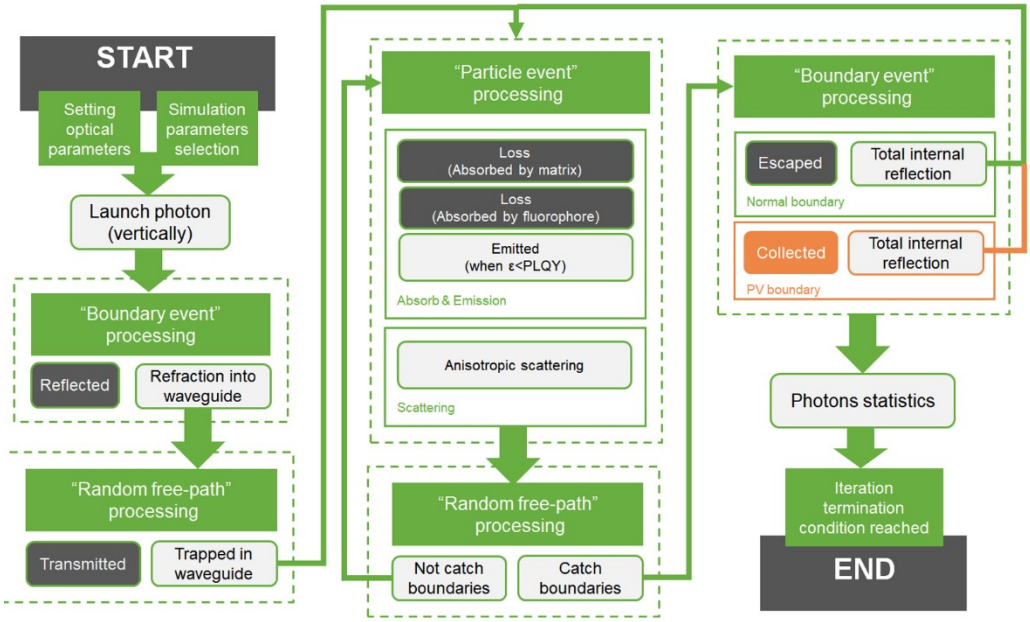

Fig. S10 Illustration of Monte Carlo ray-tracing simulated path in the FLSC. Logic flow chart of the Monte Carlo ray-tracing simulation for FLSCs.

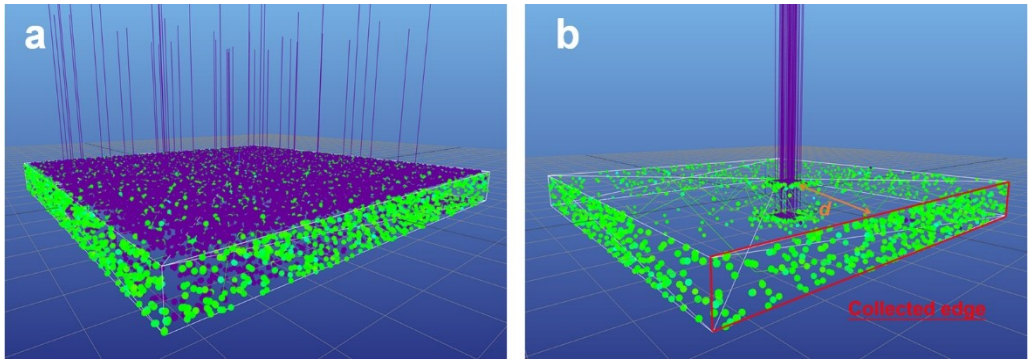

Fig. S11 Visual simulation. Constructed ray-tracing model showing a visualized representation of the fate of rays simulated within the FLSC. (a) The simulated model to calculate the PLQY, η_{edge}, η_{int} and η_{ext}. (b) The simulated model to estimate the trend of excitation distance dependent emission spectrum.

Note S7 The measurements of η_{abs} for FLSCs

There are two approaches generally used to characterize the absorptance $\eta_{abs}(\lambda)$ of the LSC. The first one is to calculate the absorptance of the LSC via $\eta_{abs}(\lambda)=1-T(\lambda)-R(\lambda)$, where $T(\lambda)$ is the transmittance, and $R(\lambda)$ is the reflectance. However, while scattering is not negligible in the FLSC, $1>\eta_{abs}(\lambda)+T(\lambda)+R(\lambda)$. The other one is to calculate the absorptance of the LSC via $\eta_{abs}(\lambda)= (1- R(\lambda)) (1-e^{-\alpha(\lambda)d})$, where $\alpha(\lambda)$ is the absorption coefficient, and d is the thickness of the LSC, and $\alpha(\lambda)=-ln(T(\lambda))/d$. But only if scattering can be ignorable in the LSC, $\eta_{abs}(\lambda)= (1- R(\lambda)) (1-e^{-\alpha(\lambda)d})$ is workable. Herein, we used an integrating sphere to directly measure the absorptance of the FLSC at the incident-light wavelength. Significantly, the incident light spot must be smaller than the top surface of the FLSC, while the incident light spot must cover the entire FLSC in the measurement of PLQY (Note S3). The $\eta_{abs}(\lambda)$ of the FLSC at the incident light wavelength can be expressed as $\eta_{abs}(\lambda)= S_{abs} /S_{inc}$ (Fig. S12).

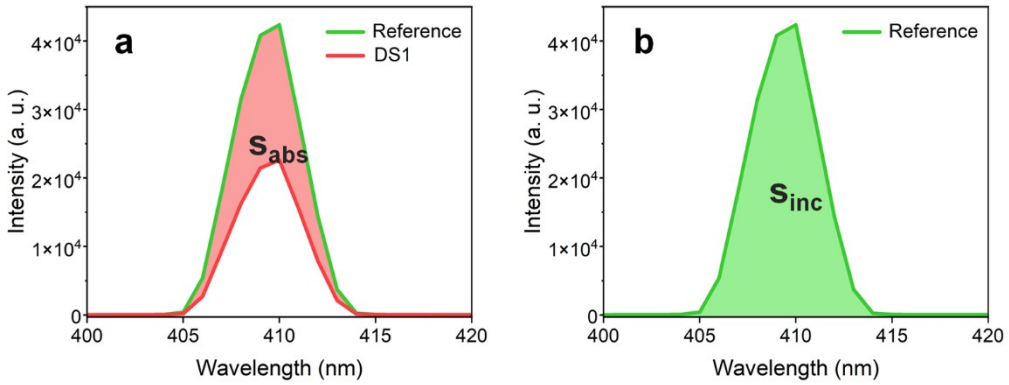

Fig. S12 Evaluation of absorptance. The filled areas (a) and the filled areas (b) of the band are proportional to, respectively, the total number of incident photons (S_{inc}) and the number of incident photons absorbed by the FLSC (S_{abs}).

Note S8 An overview of literature reports for LSCs

Table S3 An overview of literature results for LSCs*

LSC	PLQY (%)	η_{opt} (%)	LSC (cm^3)	*G*	Notes
C-dots	65	2.2	15×15×0.55	6.8	[5]
N-doped C-dots	NA	4.75	2.5×1.6×0.1	4.88	[6]
Si QDs	46	2.85	12×12×0.26	11.5	[7]
CuInSeS/ZnS QDs	40	3.3	12×12×0.3	10	[8]
$CuInSe_2$/ZnS QDs + Mn^2:CdZnS/ZnS QDs tandem	72+79	5.7	15.24×15.24×0.16 15.24×15.24×0.16	23.2	[9]
PbS/CdS QDs	45	6.1	5×1.3×0.3	10	[10]
Cs_4PbBr_6 NCs	58	2.4	10×10×0.4	6.25	[11]
$CsPbI_3$ NCs	99.4	3.1	2×2×0.2	10	[12]
$CsPbCl_3$:Mn^{2+}/Yb^{3+} QDs	125	21	12.6×12.6×0.5	6.3	[13]
Perovskite nanoplatelets	80	0.87	10×10×0.2	12.5	[14]
C-dots with Ag@SiO_2 NPs	30	0.9	5×5×0.2	25	[15]
This work	81	3.4	5×5×0.5	10	

* The η_{opt} of the LSC is estimated with an edge-mounted Si PV cell under the waveguided.

Note S9 The haze and reflectance of the FLSC and frosted glass

Total transmission (T_t) and diffusion transmission (T_d) data in Figure S13a were used to calculate the haze of DS4 sample and frosted glass in visible light. [16] A double-beam Shimadzu UV-3600 spectrophotometer with the integrating sphere was used to measure the T_t and T_d, as shown in Fig. S13b-c. These measurements were taken over the wavelength range from 380 nm to 780 nm. The haze is calculated as follows:

$$haze = \frac{T_d}{T_t}$$

The visible haze for DS4 and frosted glass are 74% and 72%, respectively. The reflectance spectra of DS4 and frosted glass are shown in Fig. S14.

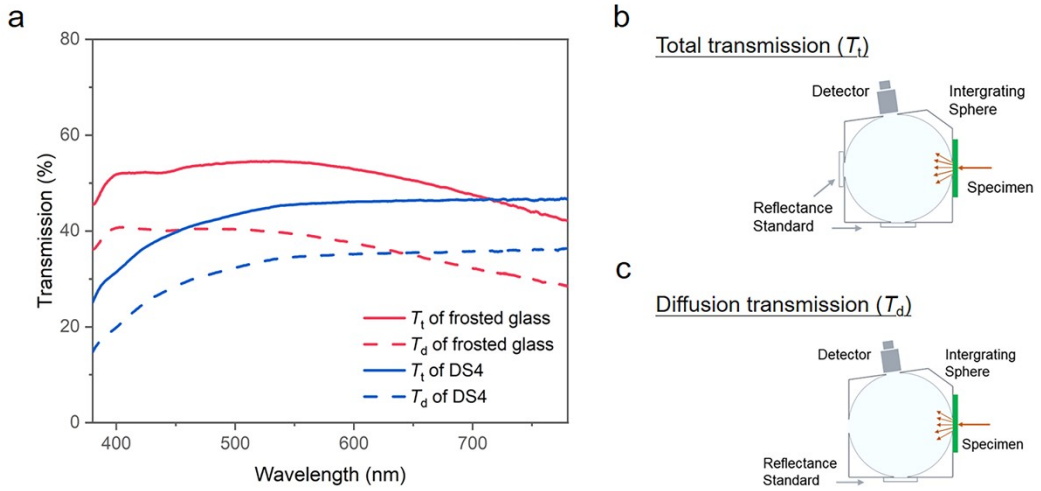

Fig. S13 (a) Total transmission and diffusion transmission spectra of DS4 and frosted glass. The schematic of the (b) total transmission and (c) diffuse transmission measurement setups.

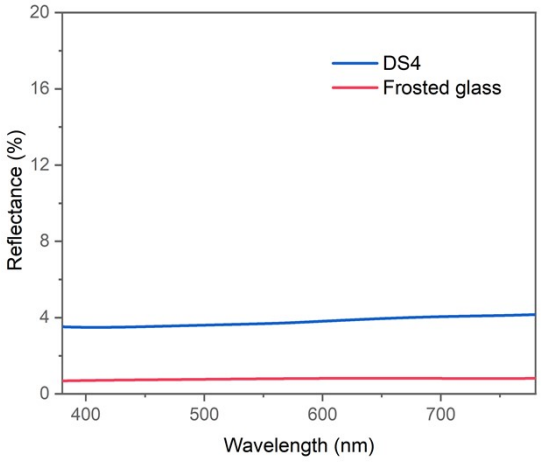

Fig. S14 Reflectance spectra of DS4 and frosted glass.

Note S10 Photostability test

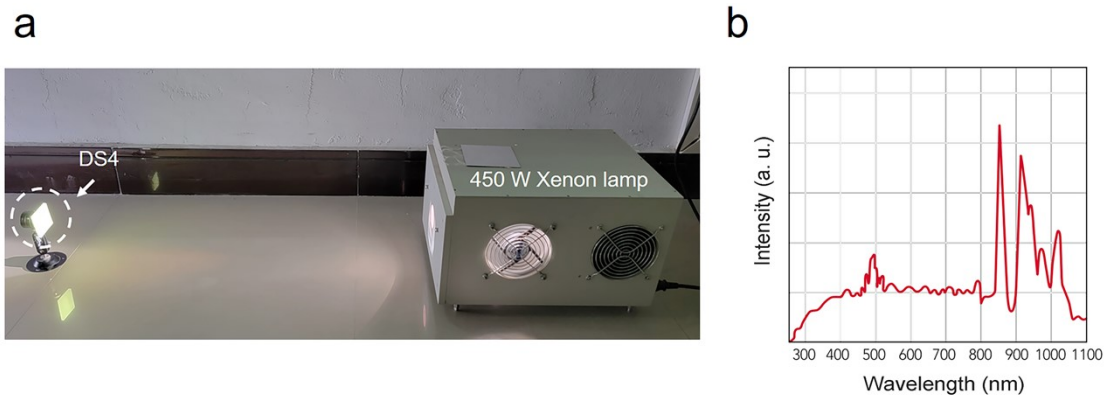

Fig. S15 (a) Photographs of DS4 irradiated by a Xenon lamp during photostability test. (b) The Xenon lamp spectrum.

Note S11 The outdoor stability test

DS4 packed into a transparent resealable bag was hung outdoors for 60 days (Fig. S16a), and the *J*-*V* characteristics of DS4 were measured under AM 1.5G illumination every 30 days (Fig. S16b). DS4 shows excellent photostability with evidence of PCE slightly decreasing from 1.37% to 1.28% and the η_{opt} decreasing from 13.2% to 11.9% for (Fig. S16c) after 438 h sunshine duration (Fig. S16d), with a big range in temperature from 16 to 38 °C and mean relative humidity from 40% to 90% (Fig. S16e-f).

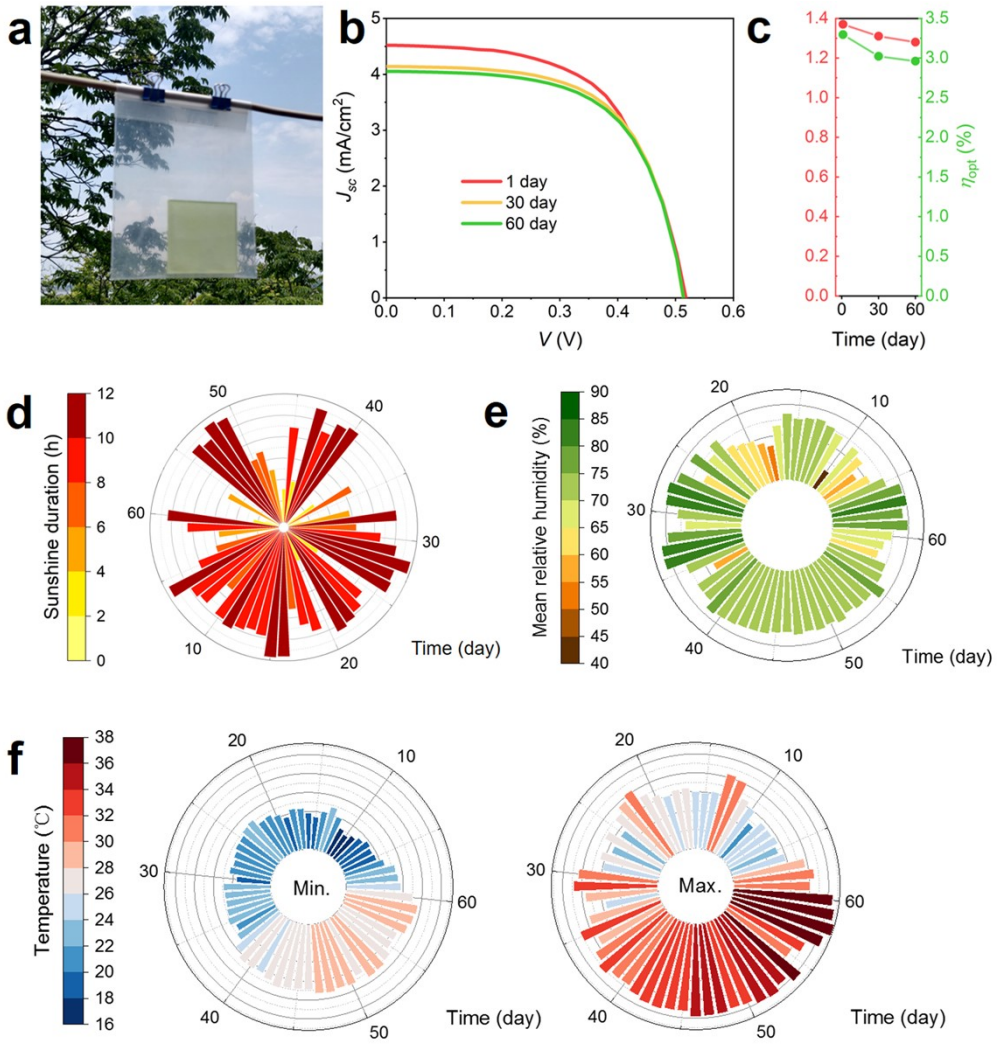

Fig. S16 Stability and long-term performance. (a) Photograph of DS4 packed and hanged outdoors. (b) *J*–*V* characteristics, (c) PCE and η_{opt} of DS4 measured under AM 1.5G illumination with edge-mounted with Si PVs during the lifetime testing. (d) Sunshine duration data, (e) mean relative humidity data, f) temperature data during lifetime testing.

Note S12 The spectrum of the UV lamp

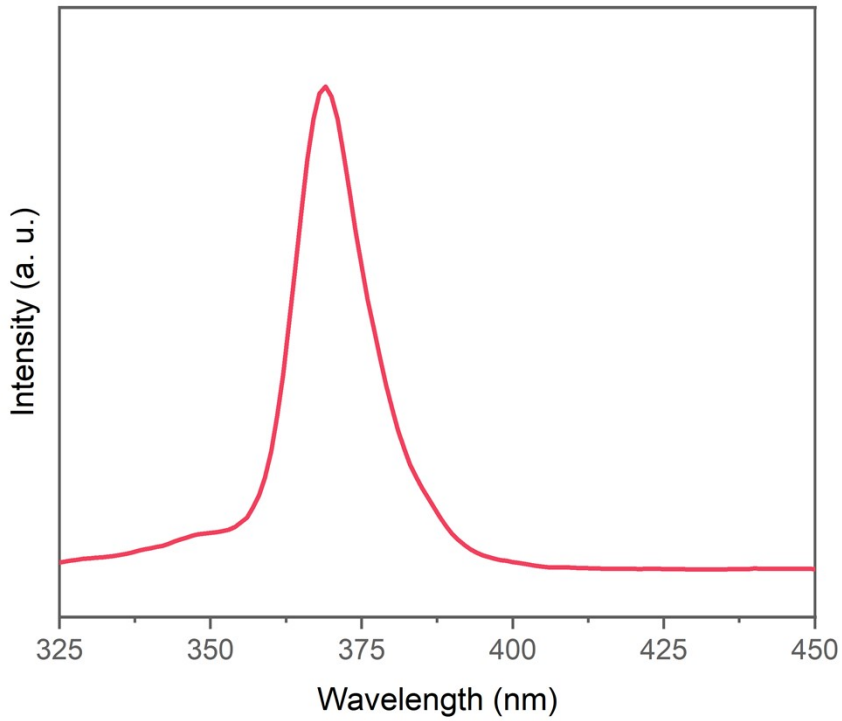

Fig. S17 Emission spectrum of the UV lamp used to cure the polymer matrix.

Note S13 The measurements of *J-V* characteristic

The Si PV strip (5×0.5 cm^2) was mounted on one waveguide edge of the FLSC with an air gap, and the remaining three edges were covered with black tapes to block the light and internal reflection of light, as shown in Fig. S18a. A matte black background was placed on the back of the FLSC to eliminate illumination from the environment or reflection. An opaque mask with well-defined area value was closely placed in front of the FLSC to block any direct illumination, as shown in Fig. S18b. The J_{SC} is calculated as follows:

$$J_{SC} = \frac{I_{Raw}(1PV)}{A_{LSC}} \times 4$$

where the I_{Raw}(1PV) is the photocurrent of the Si PV cell, A_{LSC} is the area of the waveguide front surface. The performance parameters of the Si PV strip used for photovoltaic characterization are shown in Fig. S19.

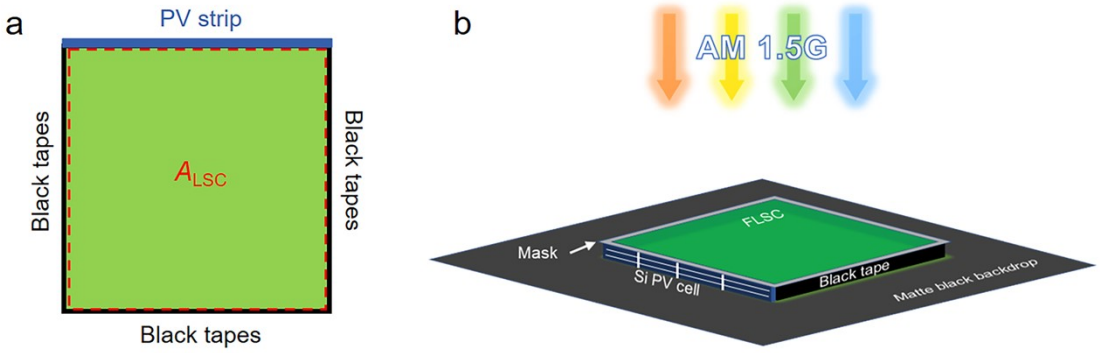

Fig. S18 (a) A schematic for the measurements of *J-V* characteristics of the FLSC. (b) A layout for *J-V* measurements for the FLSC.

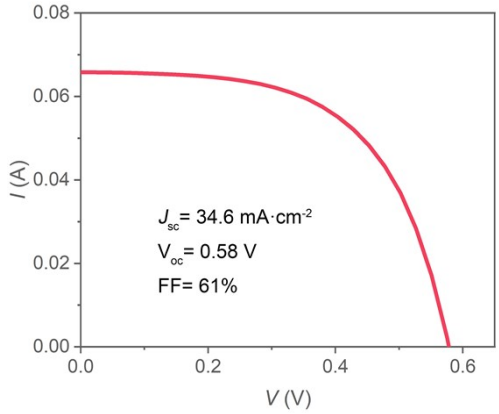

Fig. S19 *J-V* characteristic, short circuit current density, open circuit voltage and fill factor of the Si PV strip

Note S14 Optical properties of the thiol-ene polymers

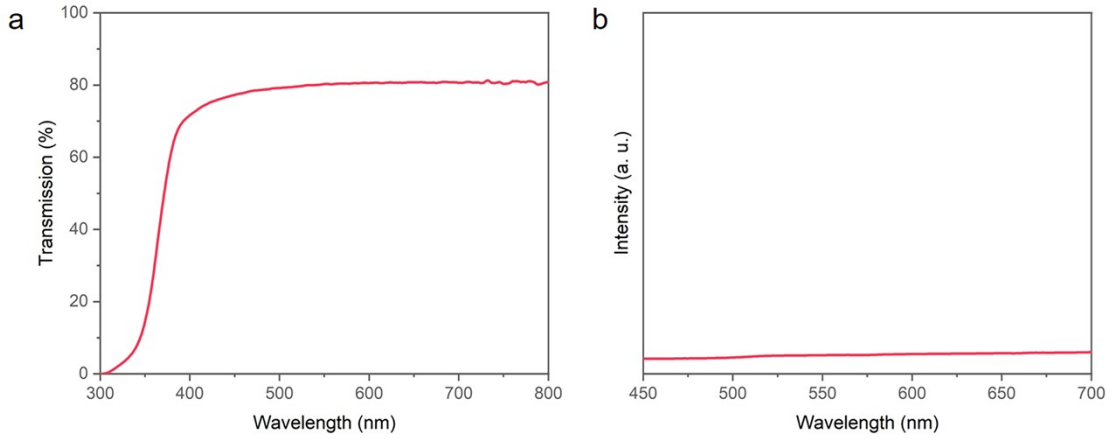

Fig. S20 (a) Transmission spectrum of thiol-ene polymers. (b) PL spectrum of thiol-ene polymers excited at 405 nm.

References

1 N. Hirosaki, R.-J. Xie, K. Kimoto, T. Sekiguchi, Y. Yamamoto, T. Suehiro and M. Mitomo, *Appl. Phys. Lett.*, 2005, **86**, 211905.

2 H. Sun, L. Pan, X. Piao and Z. Sun, *J. Mater. Chem. A*, 2013, **1**, 6388.

3 D. E. Smith, M. D. Hughes, B. Patel and D.-A. Borca-Tasciuc, *Energies*, 2021, **14**, 455.

4 D. J. Farrell and M. Yoshida, *Prog. Photovolt: Res. Appl.*, 2012, **20**, 93–99.

5 H. Zhao, G. Liu, S. You, F. V. A. Camargo, M. Zavelani-Rossi, X. Wang, C. Sun, B. Liu, Y. Zhang, G. Han, A. Vomiero and X. Gong, *Energy Environ. Sci.*, 2021, **14**, 396–406.

6 Y. Li, P. Miao, W. Zhou, X. Gong and X. Zhao, *J. Mater. Chem. A*, 2017, **5**, 21452–21459.

7 F. Meinardi, S. Ehrenberg, L. Dhamo, F. Carulli, M. Mauri, F. Bruni, R. Simonutti, U. Kortshagen and S. Brovelli, *Nature Photon*, 2017, **11**, 177–185.

8 F. Meinardi, H. McDaniel, F. Carulli, A. Colombo, K. A. Velizhanin, N. S. Makarov, R. Simonutti, V. I. Klimov and S. Brovelli, *Nature Nanotech*, 2015, **10**, 878–885.

9 K. Wu, H. Li and V. I. Klimov, *Nature Photon*, 2018, **12**, 105–110.

10 Y. Zhou, D. Benetti, Z. Fan, H. Zhao, D. Ma, A. O. Govorov, A. Vomiero and F. Rosei, *Adv. Energy Mater.*, 2016, **6**, 1501913.

11 H. Zhao, R. Sun, Z. Wang, K. Fu, X. Hu and Y. Zhang, *Adv. Funct. Mater.*, 2019, **29**, 1902262.

12 J. Wu, J. Tong, Y. Gao, A. Wang, T. Zhang, H. Tan, S. Nie and Z. Deng, *Angew. Chem. Int. Ed.*, 2020, **59**, 7738–7742.

13 T. Cai, J. Wang, W. Li, K. Hills-Kimball, H. Yang, Y. Nagaoka, Y. Yuan, R. Zia and O. Chen, *Adv. Sci.*, 2020, **7**, 2001317.

14 M. Wei, F. P. G. de Arquer, G. Walters, Z. Yang, L. N. Quan, Y. Kim, R. Sabatini, R. Quintero-Bermudez, L. Gao, J. Z. Fan, F. Fan, A. Gold-Parker, M. F. Toney and E. H. Sargent, *Nat Energy*, 2019, **4**, 197–205.

15 X. Liu, D. Benetti and F. Rosei, *J. Mater. Chem. A*, 2021, **9**, 23345–23352.

16 *Standard Test Method for Haze and Luminous Transmittance of Transparent Plastics*; West Conshohocken, PA, 2013. https://doi.org/10.1520/D1003-07E01.2.